Supporting Information

Assessment of Artificial Photosynthetic Systems for Integrated Carbon Capture and Conversion

Aditya Prajapati and Meenesh R. Singh*

Department of Chemical Engineering, University of Illinois at Chicago, Chicago, IL 60607

Email: mrsingh@uic.edu (Meenesh Singh)

Total number of pages: 30
Total number of figures: 13
Total number of tables: 6

TABLE OF CONTENTS

S1 Shockley-Queisser (SQ) Limits of Multi-junction Light Absorbers.

The SQ limits of multi-junction light absorbers can be obtained from a detailed photon balance on *n* junction light absorber, numbered in ascending order and arranged in the decreasing order of their band-gap energies from top to bottom[1-2]. The JV characteristic of the i^{th} light absorber is given by the following equation:

$$J_i = J_{\mathrm{sc},i} - J_{0,i}\left[\exp\left(\frac{eV_i}{kT}\right) - 1\right] \tag{1}$$

where J_i is the net current density, $J_{\mathrm{sc},i}$ is the short-circuit current density, V_i is the bias developed, and $J_{0,i}$ is the dark saturation current density of the i^{th} light absorber, k is the Boltzmann constant, T is the temperature, and e is the electronic charge. This current density will be the same throughout the stack of light absorbers and therefore, the individual voltages can be added up to get the total voltage. This is given by:

$$V(J) = \sum_{i=1}^{n} V_i = \frac{kT}{e}\sum_{i=1}^{n} \ln\left[\frac{J_{\mathrm{sc},i} - J}{J_{0,i}} + 1\right] \tag{2}$$

The short-circuit current density and the open-circuit voltage of a multi-junction light absorber can be obtained as:

$$\begin{aligned} J_{\mathrm{sc}} &= \min\left\{J_{\mathrm{sc},1}, J_{\mathrm{sc},2}, \ldots, J_{\mathrm{sc},n}\right\} \\ V_{\mathrm{oc}} &= \frac{kT}{e}\sum_{i=1}^{n} \ln\left[\frac{J_{\mathrm{sc},i}}{J_{0,i}} + 1\right] \end{aligned} \tag{3}$$

S1.1 JV Characteristics of Ideal Multi-Junction Light Absorbers

Fig. S1 shows the maximum current density as a function of potential across the multijunction light absorber with varying number of junctions. Fig. 2 is obtained by maximizing the current density in Eq. (2) with respect to the band-gap of each junction for a fixed potential *V*.

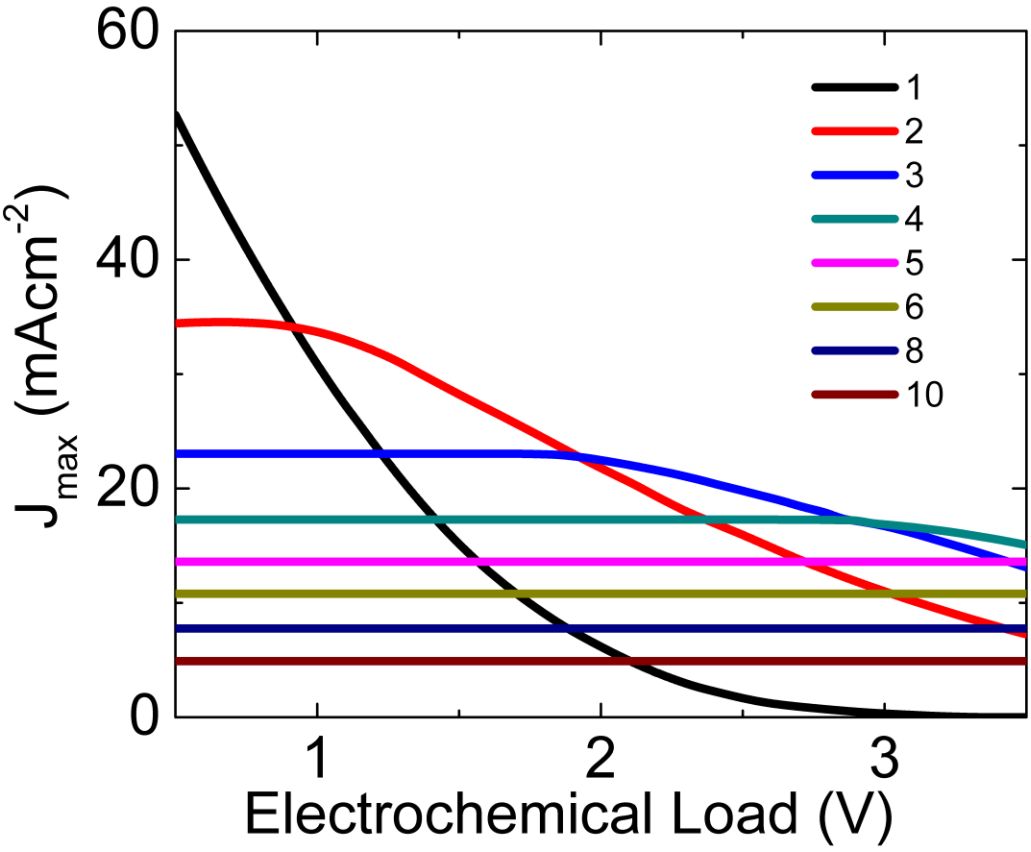

Figure S1: Maximum current density from the multi-junction light absorber versus the electrochemical load (*V*)

S1.2 JV Characteristics of a Real Triple-Junction Light Absorber

A measured JV characteristic of Spectrolab's most efficient InGaP/GaAs/Ge [3] triple-junction light absorber under 1 sun and AM 1.5 is shown in Figure S2.

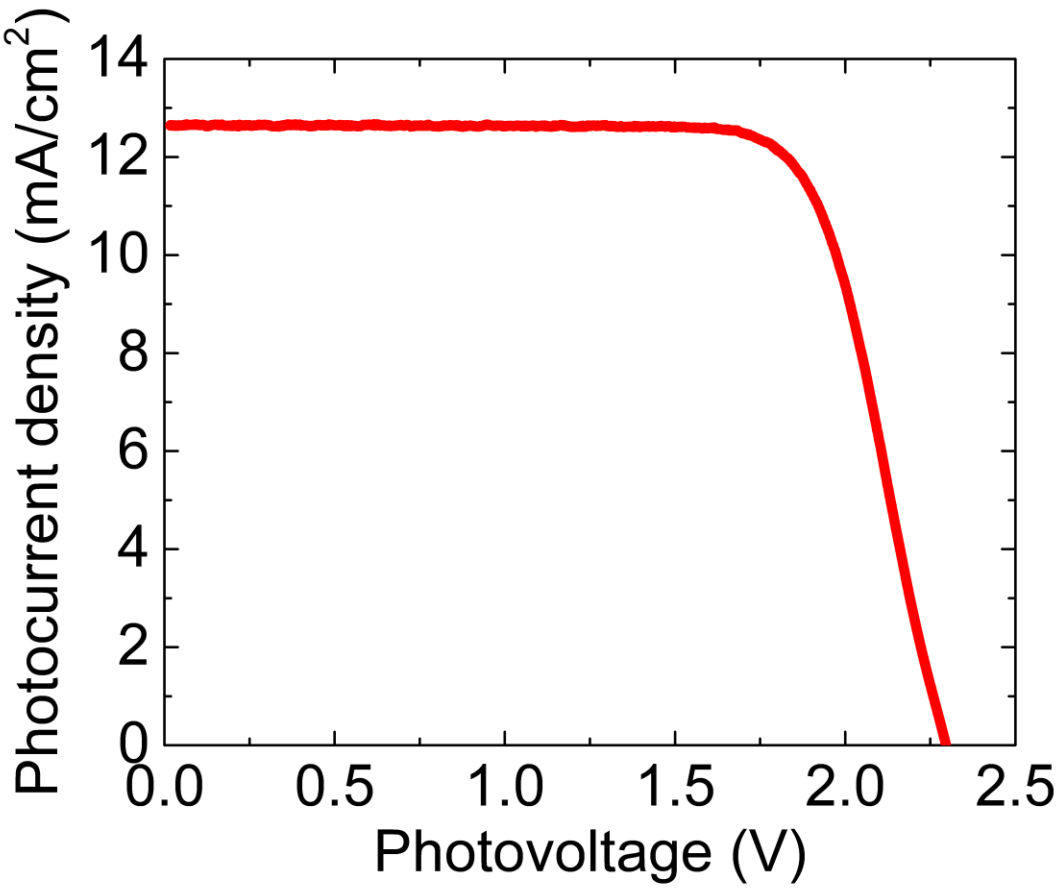

Figure S2: JV characteristics of InGaP/GaAs/Ge under 1 sun at A.M. 1.5

S2 Optimal Band-Gaps for Multi-Junction Light Absorbers

Figure S 3 shows the optimal band-gaps of single-, double-, triple-, and quadruple-junction light absorbers as a function of applied potential. These band-gaps are optimized to obtain maximum current density from the multi-junction light absorbers. The band-gap for a single-junction light absorber increases at the rate of 1.06 eV/V. This causes a decrease in the fraction of the solar spectrum absorbed and, therefore, in the current density at higher electrochemical load. The optimal band-gaps for the top and the bottom junctions of a double-junction light absorber remain constant till a load of 0.9 V and then increase linearly at a rate of 0.42 and 0.62 eV/V respectively. The top, middle, and the bottom junctions of a triple-junction light absorber remain at a constant value up to a load of 1.8 V and then increase at the rates 0.22, 0.31, and 0.5 eV/V respectively. For a quadruple-junction light absorber, the top, upper-middle, lower-middle, and the bottom junctions remain constant up to a load of 2.85 V and thereafter increase at a linear rate of 0.12, 0.15, 0.16, and 0.44 respectively.

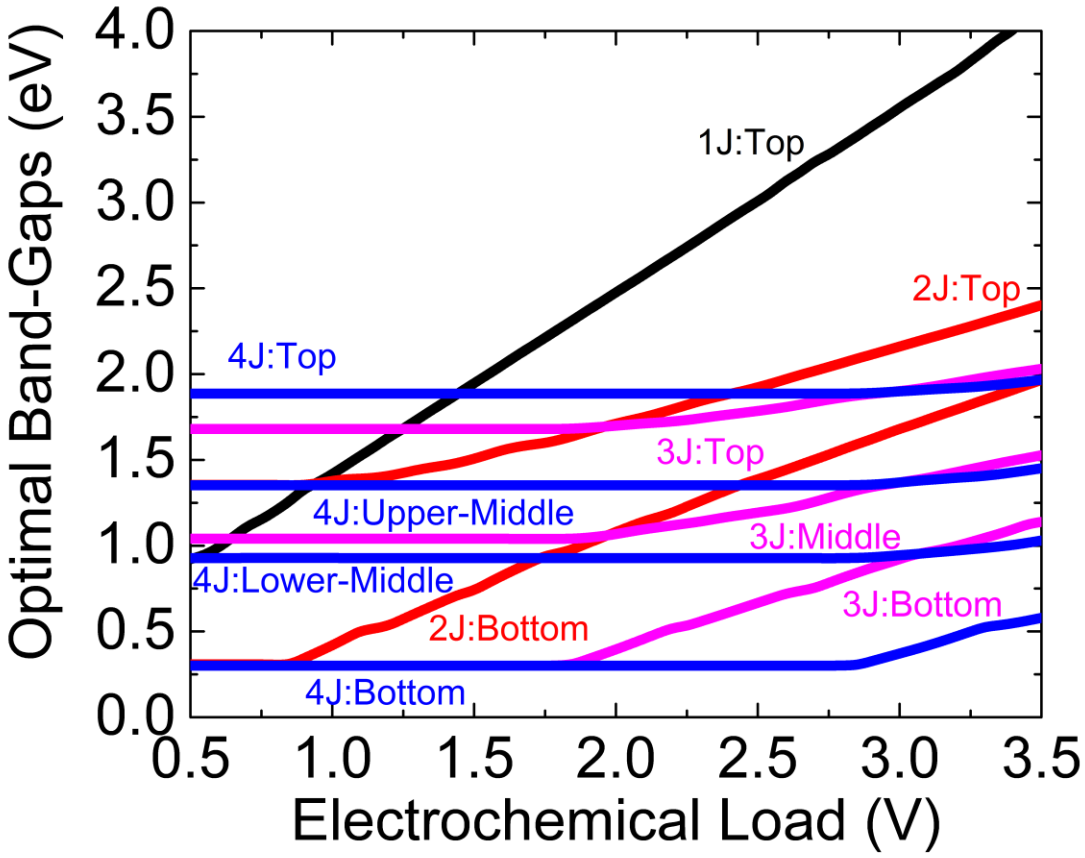

Figure S 3 Optimal band-gaps of a single- (black), double- (red), triple- (magenta), and quadruple- (blue) junction light absorber for various electrochemical loads.

S3 Thermoneutral Potentials of CO_2 Reduction Products

Table S1 shows the thermoneutral potentials of the CO_2 reduction products based on their higher heating values and the lower heating values.

Table S1: Thermoneutral potentials for various CO_2 reduction products

Products	No. of electrons	HHV (kJ/mol)	$U_{H,\,HHV}$ (V)	E^0 (V)	LHV (kJ/mol)	$U_{H,\,LHV}$ (V)
H_2	2	285.8	1.482	1.229	241.81	1.254
CO	2	282.98	1.467	1.329	282.98	1.467
HCOOH	2	253.81	1.316	1.249	209.82	1.088
CH_3OH	6	726.71	1.256	1.199	638.73	1.104
CH_4	8	890.24	1.154	1.059	802.23	1.04
C_2H_5OH	12	1367.42	1.182	1.144	1235.45	1.068
C_2H_4	12	1410.92	1.219	1.149	1322.94	1.143

S4 Carbon Capture Processes

Various carbon capture processes were considered in Table 1 of the manuscript to evaluate the energy requirement. The mechanisms of each of the processes are briefly discussed in this section.

Mechanism of CO_2 Capture Processes

Ideal CO_2 capture: This is an ideal process considered for a reference to compare the energy consumption of all the realistic/conventional carbon capture processes. It is a reversible process in which the CO_2 is captured and concentrated from a dilute source (air, or flue gas). The energy required for this process is given by the free energy change of concentrating CO_2 from a lower concentration of a dilute source to ~100%, such that

$$\Delta G = -RT \ln\left(\frac{p}{p_0}\right) \tag{4}$$

where p is the partial pressure of CO_2 (which varies depending on the source of CO_2) and p_0 is the atmospheric pressure assuming pure stream of CO_2. Here we have assumed ideal behavior of CO_2 gas.

Liquid absorption using NaOH*:* In this process, CO_2 is captured by spraying NaOH[4] through the passing stream of gas where CO_2 is absorbed and a solution of Na_2CO_3 forms. NaOH is regenerated from Na_2CO_3 by addition of lime which forms $CaCO_3$. $CaCO_3$ is then decomposed back to CaO by the application of heat.

Liquid Absorption using Monoethanolamine: This process is conventionally used to capture CO_2[5] from a flue gas stream using monoethanolamine (MEA). Figure S 4 describes the mechanism of CO_2 capture using MEA, which starts with the formation of carbamate formation in the initial stage. This is a reversible exothermic process when there is a lower loading of CO_2. The pH of the CO_2-MEA solution decreases with increasing loading of CO_2 in the MEA. As the loading of CO_2 increases, the formation of carbamate becomes a weaker step in the mechanism and is followed by the hydration of CO_2 where it forms a mixture of HCO_3^-/CO_3^{2-}.

Industrially, MEA technology is used for a post-combustion CO_2 capture as such a scheme is easier to implement and can be retrofitted to the already existing CO_2 emitters. One of the prominent uses of MEA is to capture CO_2 from the flue gas in the coal-fired power plant. A typical MEA unit contains a 25-30 wt% MEA in water and is fed with the flue gas in a temperature range of 25-40 ^oC. For a rich loading (~0.5 mol CO_2/ mol MEA), maximum rate of absorption of CO_2 is 1.52 $mmols^{-1}m^{-2}$ with a maximum absorption capacity of 49-50%.[6] The solvent is then regenerated by heating the solution to ~90 ^oC. This regeneration technique is highly energy intensive as MEA goes under thermal and oxidative degradation and requires a large solvent makeup.[7] As the regeneration of MEA releases CO_2, there is a need for an additional compressor unit which accounts for additional cost to this technology. Table S5 shows the operating cost of an MEA unit to be \$49/ton of CO_2.

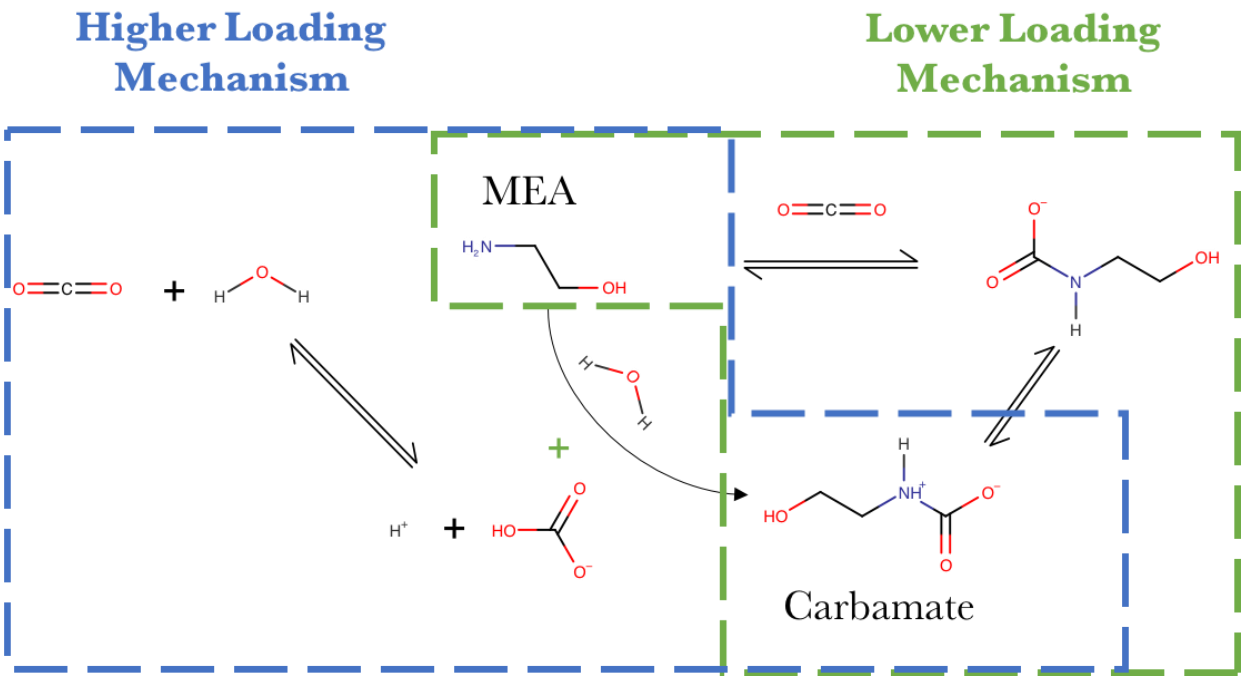

Figure S 4 CO_2 capture and solvent recovery mechanism using MEA

Solid adsorption using Metal-Organic Frameworks (MOFs): MOF sorbents are a relatively new class of solid adsorbents and they capture CO_2 by physisorption[7]. A generalized physisorption mechanism of CO_2 capture can be given by:

$$CO_2 + (active\ site) \rightarrow CO_2 * (active\ site)$$

MOFs are composed of metal ions or metal cluster vertices linked by organic spacers (functional groups). MOFs are versatile solid adsorbents due to the two of their most important features: 1) MOFs can be synthesized in different modules giving great control over the selection of functional groups comprising the organic linkers to vary MOF properties like pore size, shape, and selectivity towards CO_2. 2) MOFs are crystalline solids. The crystallinity makes it easier to completely characterize a MOF crystal using XRD which greatly facilitates designing different MOFs with the precise details of the atomic coordinates of the frameworks. The heat of adsorption ranging up to 90 kJ/mol of CO_2 have been observed in MOFs (Table 1 of the manuscript). There are MOFs which exhibit even higher heats of adsorption however, such strongly binding MOFs are not favorable because a higher amount of energy is needed to recover CO_2.

Solid Adsorption using K_2CO_3: Alkali metal carbonates are widely studied to capture CO_2. K_2CO_3 is stable over a wider range of temperature compared to Na_2CO_3 and Li_2CO_3 and hence is a stronger candidate as a solid sorbent for CO_2 capture. Usually, K_2CO_3 is coated on porous support like activated carbon[8] to enhance the contact area with CO_2. K_2CO_3 captures CO_2[9] in the presence of moisture by the following reaction:

$$K_2CO_3 + CO_2 + H_2O \rightleftharpoons 2KHCO_3$$

A typical CO_2 capture unit using solid adsorbents comprises of two fluidized bed reactors containing the spent and the regenerated adsorbent as seen in Fig 1(B) of the manuscript. The

fluidized beds are used because they exhibit enhanced gas-solid mixing and uniform temperature distribution throughout the reactor. The flue gas is sparged at the bottom of the first fluidized bed containing the fresh adsorbent. The operating temperature is usually the temperature at which the adsorbent has the maximum CO_2 capture capacity (2.13 mmol/g of sorbent around 100-110 ^oC)[8, 10]. Once the adsorbent has reached its capacity, it is transferred to the regeneration column where heating the adsorbent releases pure CO_2. The regeneration temperature of the adsorbent can vary depending on the support material used. For porous support like activated carbon, the adsorbent can be fully regenerated at a temperature of 150 ^oC without losing the carbon capture capacity up to 10 cycles of adsorption and regeneration.[8] The cost of operating of an adsorption based CO_2 capture unit is $ 57/ton CO_2 (Table S5).

Moisture-swing Absorption Membrane: The mechanism of the moisture-swing absorption of CO_2 on a quaternary amine-based resin membrane is shown in Figure S 5. The quaternary amines are attached to a polystyrene backbone have hydroxide, carbonate, or bicarbonate counter ions which help the resin to sustain sufficiently high pH conditions to enable a direct CO_2 capture from air. The hydroxyl functional groups attached to the dry-side of the resin surface can react with CO_2 to form bicarbonates. The absorption/desorption mechanism can be described by the following reactions:

Step1: $$OH^- + CO_2 \rightarrow HCO_3^-$$

Step2: $$CO_3^{2-} + H_2O + CO_2 \rightleftharpoons 2HCO_3^-$$

Step3: $$OH^- + HCO_3^- \rightleftharpoons CO_3^{2-} + H_2O$$

Step 1 is dominant on the dry-side and CO_2 will be captured as long as there are hydroxyl groups available for the reaction forming high concentrations of bicarbonates. On the wet-side of the resin, however, the availability of the H_2O species shifts the carbonate and bicarbonate equilibrium in the opposite direction and the reverse reaction of Step 2 will be dominant resulting in the release of CO_2. [11]. The physics of this membrane is used to model the integrated CO_2 capture and reduction system shown in Fig 1C of the manuscript.

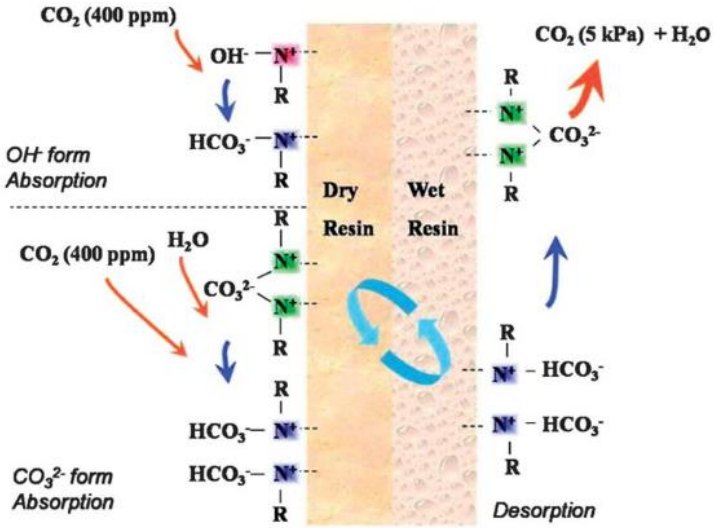

Figure S 5 Mechanism of moisture-swing absorption of CO_2. This figure is adapted from Ref [11].

For continuous operation of an integrated system using this membrane to capture CO_2, it is important to determine the JV characteristics of this process to see its effect on the overall solar-to-fuel (STF) efficiency. It can be seen from the step 2 of the absorption/desorption mechanism that the flux of water plays an important role in shifting the equilibrium on the wet-side of the resin membrane to release the CO_2 which is given by

$$N_w = \frac{D_w}{L}(C_{wet} - C_{dry}) \quad (5)$$

where D_w is the diffusion coefficient of water, L is the thickness of the membrane, C_{wet} is the concentration of water at the wet-side (~12.5 M for 100% relative humidity), and C_{dry} is the concentration of water at the dry-side. Using the water sorption isotherm of the anion-exchange membrane,[12-13] the concentration of water on the dry-side is calculated to be 2 M for a relative humidity of 40%. For a fixed flux of water through the resin, the rate at which the energy is consumed to condense water coming out of the resin is given by

$$E_c = N_w \times \lambda_w \quad (6)$$

where λ_w is the latent heat of water. This value of energy consumption depends on the flux of water which in turn depends on the relative humidity on the dry-side of the resin. Since the flux of water and CO_2 are related in Step 2, the energy consumed per mole of CO_2 captured (or carbon capture potential) is independent of the water flux. The physics of this membrane was simulated at varying current densities for a 0.1mm thick anion-exchange resin membrane (1M ion-exchange capacity) with a well-mixed electrolyte on the wet-side and the dehumidified air on the dry-side by solving equations (9)-(26) using COMSOL Multiphysics. Figure S 6 shows the concentration profile of various species across the membrane obtained at a current density of 1 mA cm^{-2}. These concentration profiles agree with the above-mentioned absorption/desorption mechanism.

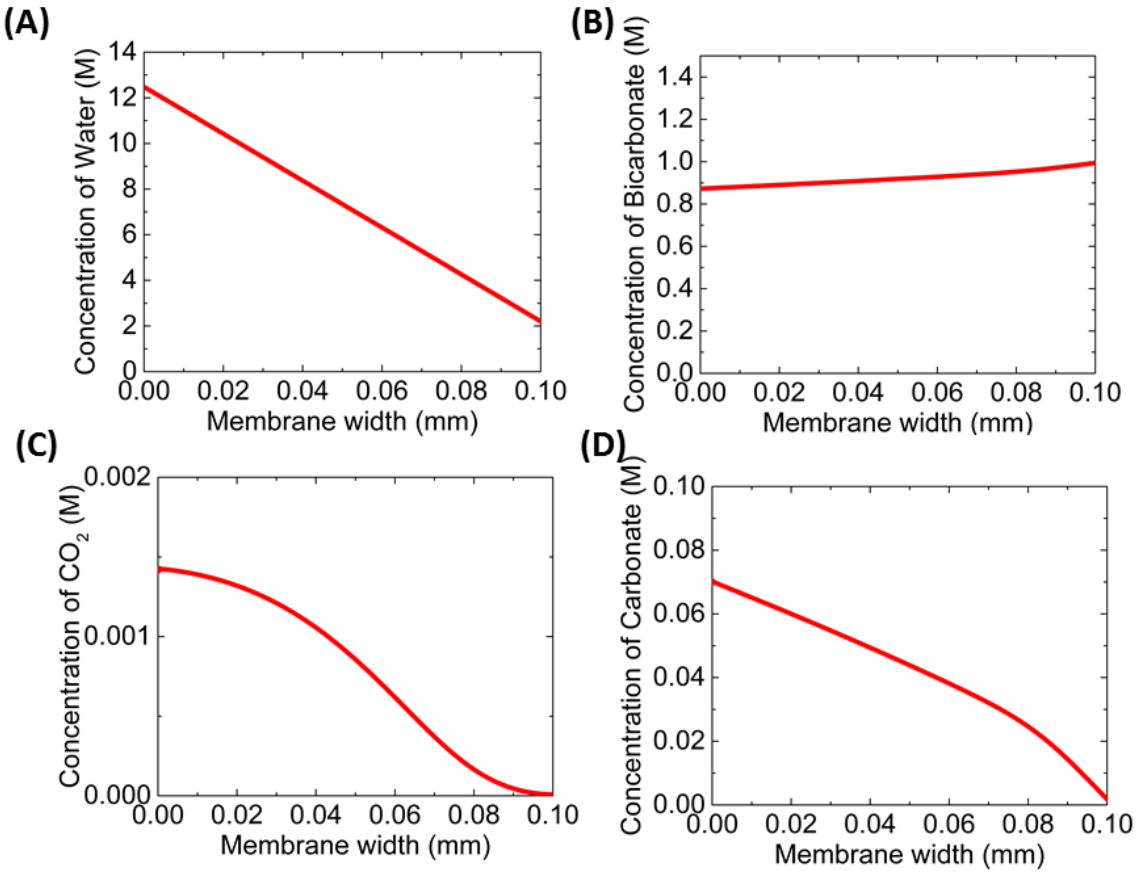

Figure S 6 Concentration profiles across the membrane of 0.1 mm thickness at a current density of 1 mA cm^{-2} of (A) Water, (B) Bicarbonate ions (C) CO_2, and (D) Carbonate ions.

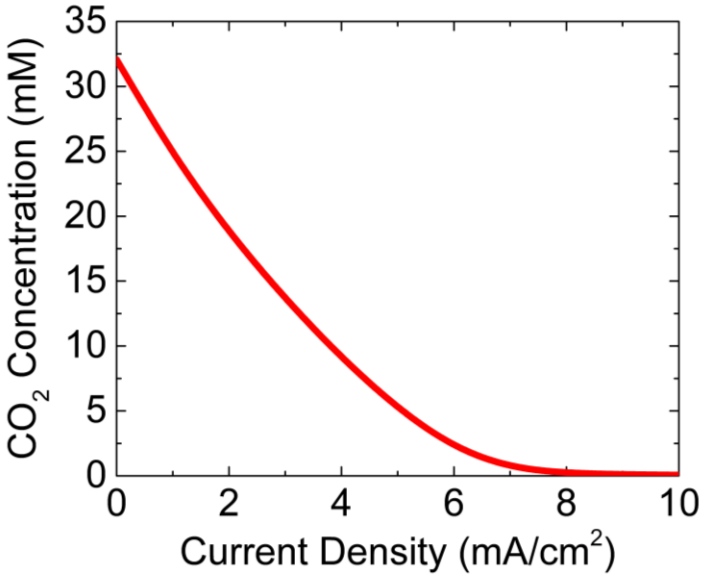

Figure S 7 Effect of current density on the CO_2 concentration in the well-mixed electrolyte

Figure S 7 shows the effect of current density on the CO_2 concentration in the well-mixed electrolyte. At the equilibrium in absence of current density, CO_2 is at its maximum concentration at standard conditions of ~33mM which can be obtained by Henry's law. The CO_2 concentration in the electrolyte decreases with increasing the current density of CO_2 reduction reaction for a fixed flux of water across the resin. Since the flux of water from the resin and hence the power required to condense water is constant for a varying current density in Fig. S7, the JV characteristic for CO_2 capture using anion-exchange resin will be a vertical line.

Lackner in 2009[14] proposed a design of a prototype for such a device for capturing one ton of CO_2 per day from the air. The device was envisioned to be modular involving a set of air filters $2.5m \times 1m \times 0.4m$ with the air flow speed of 1 m/sec. The entire system for the desired capacity would contain 60 such units. The total volume of these units would be stored in a standard shipping container of dimensions $12m \times 2.5m \times 3m$.

A single membrane filter takes approximately one hour to get saturated with CO_2. Once it has been saturated, it is then removed from the air collector and placed into an evacuation chamber. Filters from all the units are collected in such evacuation chambers (10 filters per chamber) where the air is pulled out by vacuum. The CO_2 is then released from these membrane filters by injecting moisture. The target of this prototype was to build up a CO_2 partial pressure between 5 and 10 kPa which can be compressed subsequently resulting in heat release due to moisture condensation. Energy is consumed by three major components: 1) Removal of air from the evacuation chamber consumes 4 kJ/mol for 0.25 mol CO_2/kg resin loading, 2) CO_2 compression from 5kPa to 6.7MPa at 300K to obtain liquid CO_2 requires 19kJ/mol, and 3) The condensation of water consumes 2.5 kJ/mol of water. The cost of operation of such membrane units to capture 1-ton CO_2/day is $30/ton CO_2 (Table S5).

Electrodialysis: This process uses bipolar membrane electrodialysis (BPMED) to extract CO_2 dissolved in seawater. Figure S 8 shows the schematic of the electrodialysis setup. The input seawater stream is electrodialysed into two separate acidic and alkaline streams. The dissolved CO_2 in the acidic stream is subsequently vacuum stripped using the membrane contactors. Finally, the acidic and the basic streams are merged together in a waste collection tank.

The energy consumption for electrodialysis reported in Table 1 of the manuscript is independent of the rate of CO_2 capture, which can be seen in Figure S 9 showing that the JV characteristics for the electrodialysis process derived from the experimental data.[15] At various CO_2 currents, the value of carbon capture potential remains almost constant and the graph is a vertical line. Hence, the energy consumption may be considered independent of the rate of CO_2 capture.

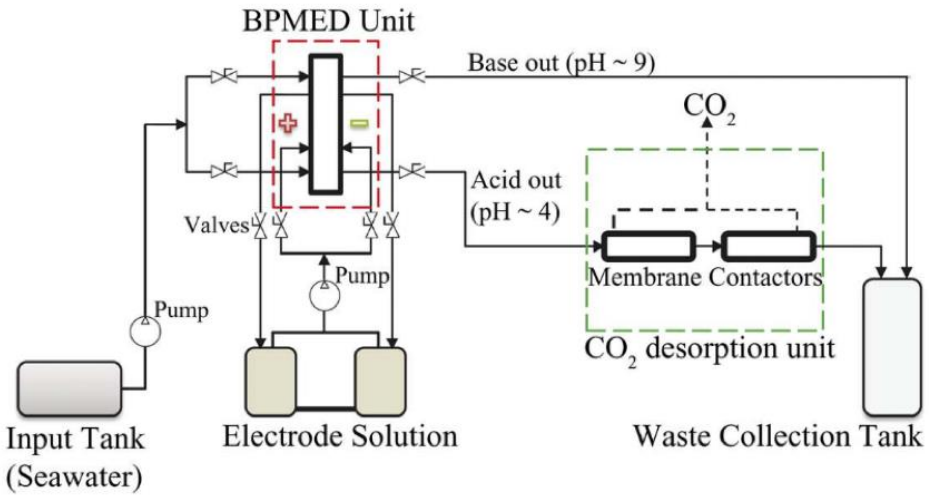

Figure S 8 Schematic diagram of bipolar membrane electrodialysis (BPMED) process[15]

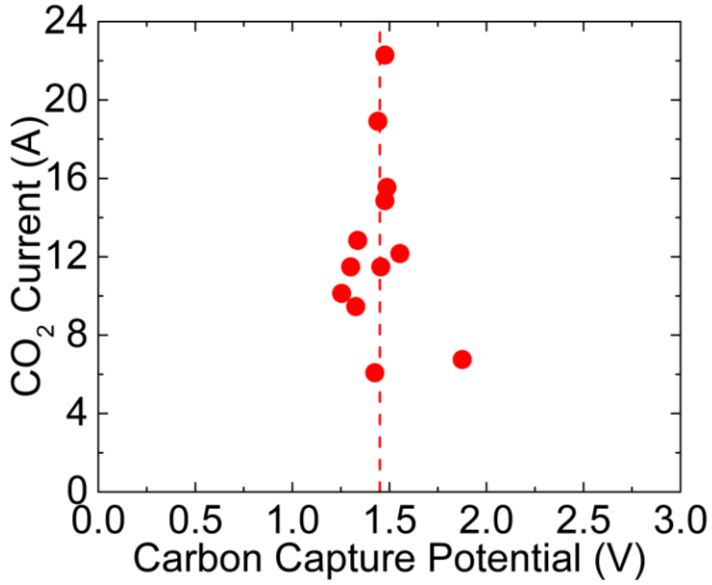

Figure S 9 Measured JV characteristics of CO_2 capture by BPMED of seawater

Eisaman et al.[15] constructed a nine-cell series stacked arrangement with each cell consisting of a CEM, basic compartment, BPM, acidic compartment, and an AEM. The active area of each of the membranes is 180 cm^2. The experiment to extract CO_2 from seawater was done at various flow rates of seawater with 6 lpm being the highest. The seawater and the acidic and the basic solutions flow through the stacked cells at the same flow rate to prevent any inter-compartmental pressure drops. The vacuum pump at the headspace of the acidic compartment is then turned on and the CO_2 dissolved in the seawater is extracted from the acidic compartment. The rate of CO_2 extraction is dependent on the pH of the acidic compartment. As the pH in the acidic compartment drops, the rate of CO_2 extraction increases until the solution pH and the CO_2 extraction rate reach steady-state values. The highest rate of CO_2 extraction at 6 lpm was around 0.3 slpm at the pH ~3.5. The CO_2 extraction from this experimental setup was observed to be 68% at 6 lpm. The cost of operation to extract 1-ton CO_2/day was calculated to be \$394.41/ton CO_2 (Table S5)

S5 Solar-to-fuel (STF) Efficiency of AP Systems with Ideal Light Absorbers

Figure S 10 shows the STF efficiency of CO_2 reduction products as a function of the energy of carbon capture for multi-junction light absorbers with the number of junctions varying from 4 to 10. It can be seen from the figure that all the products show a constant STF efficiency. The difference between the STF efficiencies of each product is due to the difference in their thermoneutral potential. The constant STF efficiency with respect to the energy of carbon capture is a result of the light absorbers being able to absorb a broader spectrum of light. The decrease in the STF efficiency with the increasing number of junctions is due to the current mismatch between the junctions.

Figure S 11 shows the STF efficiency of each CO_2 reduction product for various multi-junction light absorbers. As the number of junctions increases, the overall STF efficiency decreases and as the number of junctions increases beyond 3, the STF efficiencies for all the CO_2 reduction products becomes insensitive to the capture processes used. The light absorbers with a higher number of junctions have a constant maximum current density for a wider range of electrochemical load (Figure S1) and hence, the choice of carbon capture process does not affect the STF efficiency as the number of junctions in a light absorber become greater than 3.

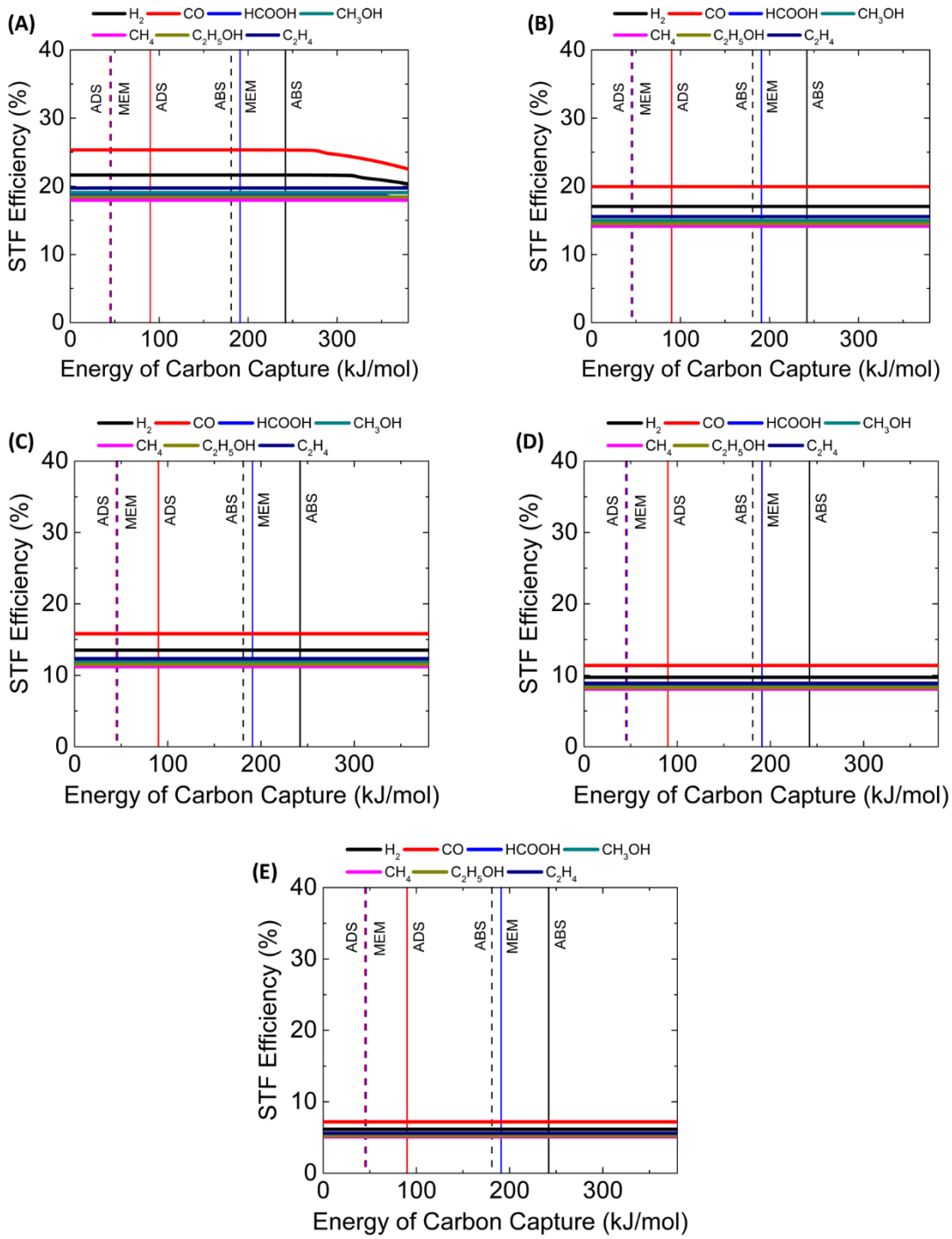

Figure S 10 STF of H_2, CO, HCOOH, CH_3OH, CH_4, C_2H_5OH, C_2H_4 versus energy of carbon capture for (A) quadruple junction, (B) quintuple junction, and (C) sextuple junction (D) octuple (E) decuple light absorbers.

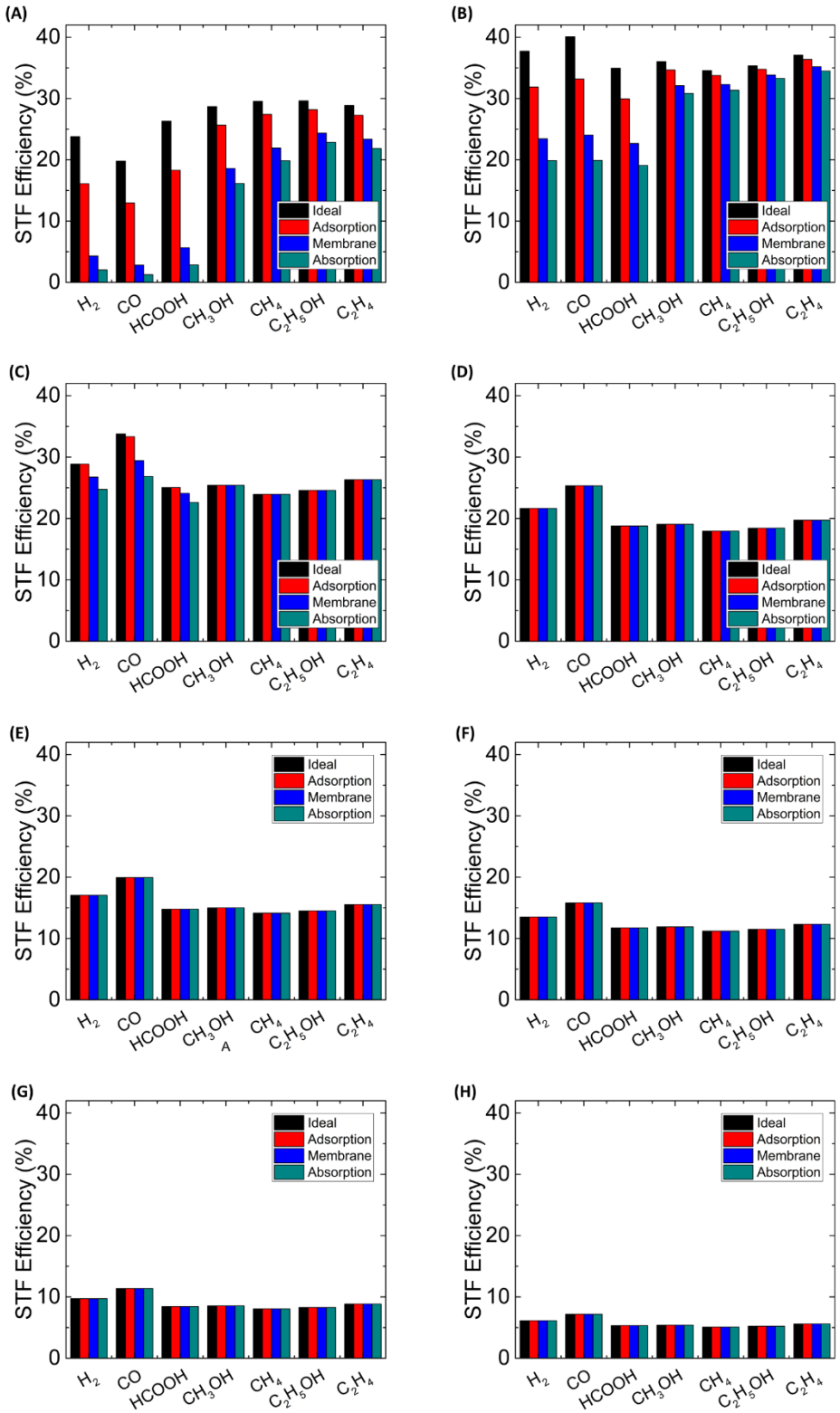

Figure S 11 STF efficiency of different CO_2 reduction products for different CO_2 capture processes for (A) single-junction, (B) double-junction, (C) triple-junction, (D) quadruple-junction, (E) quintuple-junction, (F) sextuple junction, (G) octuple-junction ,and (H) decuple light absorbers.

Figure S 12 is a corollary of Figure S 10 and Figure S 11 which shows the dependency of the STF efficiency on the number of light absorber junctions for an integrated system where the CO_2 is captured from air using various processes and is reduced to CH_3OH and CO. There is an increase in the efficiency from a single- to a double-junction light absorber for both the products which is accounted for by the increase in the absorption spectrum of the double-junction light absorber. As the number of junctions becomes >3, the STF efficiency of the CO_2RR products lose their sensitivity to the carbon capture processes and the STF efficiency is mainly determined by the thermoneutral potential of the products as the maximum photocurrent current density is constant.

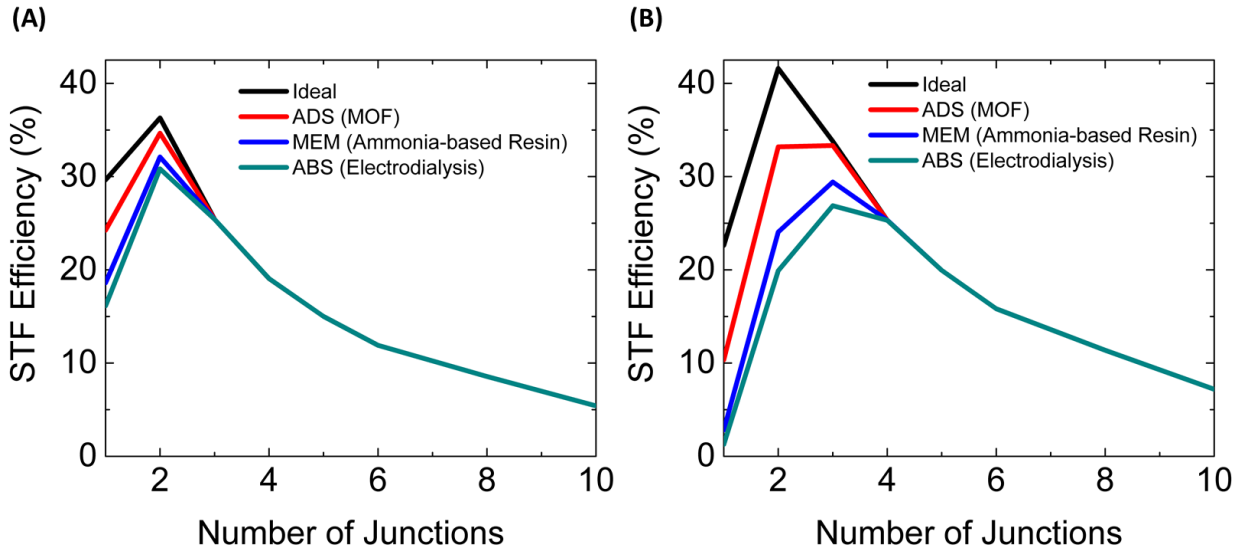

Figure S 12 Dependence of STF efficiency on the number of junctions of a light absorber for an integrated AP system with CO_2 capture (from air) and reduction to (A) CH_3OH, and (B) CO

S6 Mass Transfer Effects on the Total Current Density

The availability of concentrated CO_2 supply for an integrated AP system is crucial for achieving high STF efficiency. However, this efficiency is significantly affected due to the limitations imposed by the mass transfer of CO_2 in the gas phase. Hence, it is important to evaluate the mass transfer effects on the total current density.

The effect of mass transfer on the total current density was studied for an integrated AP system shown in Fig. 1C of the manuscript. The CO_2 mass transfer coefficient at the boundary was determined by the correlation:

$$\mathrm{Sh} = 2 + 0.6 \times \mathrm{Re}^{\frac{1}{2}} \mathrm{Sc}^{\frac{1}{3}} \tag{7}$$

where Sh is the Sherwood number, Re is the Reynolds number, and Sc is the Schmidt number. The mass transfer coefficient was obtained using the above correlation for the gas velocity of 1 cm/s. The limiting current density was determined as follows:

$$J_{lim} = nFk_g c_{CO_2} \tag{8}$$

where J_{lim} is the limiting current, n is the number of electrons transferred, F is the Faraday's constant, k_g is the mass transfer coefficient and c_{CO_2} is the concentration in the feed stream to the integrated AP system.

S7 COMSOL Model for a CO_2 Distribution in a Fully Integrated AP System

A two-dimensional electrochemical cell for a fully integrated CO_2 capture and reduction was developed to determine the current density and the distribution of CO_2 in such a system. The Pt anode is used for water oxidation and nanoporous Ag cathode is used for CO_2 reduction. The anolyte and catholyte are separated by an anion-exchange membrane such as Selemion of 100 μm thickness. The species in the CO_2 equilibrated electrolyte are dissolved CO_2, bicarbonate anions (HCO_3^-), carbonate anions (CO_3^{2-}), protons (H^+), hydroxide anions (OH^-), and potassium ions (K^+). The pH of the electrolyte is 6.8 and the initial concentration of potassium ions is 0.1 M.

Polarization Losses

Polarization loss due to transport of species (by migration and diffusion) and concentration gradients can be represented as a sum of i) ohmic loss, ii) diffusion loss, and iii) Nernstian loss. The ohmic loss is due to the resistance of the electrolyte, and the diffusion loss originates from the ionic gradient in the boundary layer near each electrode due to the applied current density. The ohmic and diffusion losses can be combined into the solution loss such that

$$\Delta\phi_{\text{solution}} = \underbrace{\int \frac{i_l}{\kappa} dx}_{\Delta\phi_{\text{ohmic}}} + \underbrace{\sum_i \int \frac{Fz_i D_i \nabla c_i}{\kappa} dx}_{\Delta\phi_{\text{diffusion}}} \tag{9}$$

where i_l is the electrolyte current density, κ is the electrolyte conductivity, x is the position, F is Faraday's constant, z_i is the charge number, D_i is the diffusion coefficient, and c_i is the concentration of the i^{th} species. The ionic gradients alter the concentrations of reacting species next to the electrode surfaces (e.g., protons, hydroxide anion, and dissolved carbon dioxide) away from those present in the bulk. This causes an increase in the equilibrium potential of the oxygen evolution reaction (OER) and the carbon dioxide reduction reaction (CO2RR), which are referred to collectively as the Nernstian loss. The Nernstian loss is a sum of losses due to differences in pH at the two electrodes, and differences in concentration of carbon dioxide at the cathode and in the bulk electrolyte is given by

$$\Delta\phi_{\text{Nernstian}} = \underbrace{\frac{2.303RT}{F}\left(\text{pH}_{\text{cathode}} - \text{pH}_{\text{bulk}}\right)}_{\Delta\phi_{\text{cathode pH}}} + \underbrace{\frac{2.303RT}{F}\left(\text{pH}_{\text{bulk}} - \text{pH}_{\text{anode}}\right)}_{\Delta\phi_{\text{anode pH}}} + \underbrace{\frac{RT}{nF}\ln\left(\frac{p_{\text{CO}_2,\text{ bulk}}}{p_{\text{CO}_2,\text{ cathode}}}\right)}_{\Delta\phi_{\text{cathode CO}_2}} \tag{10}$$

where R is the gas constant, T is the temperature, n is the moles of electron transferred per mole of CO_2, and p_{CO_2} is the partial pressure of carbon dioxide. The losses given by equations (9) and (10) are due to transport of species in the electrolyte, which, in turn, depend on the applied current density, electrolyte composition, electrolyte hydrodynamics, carbon dioxide feed concentration and rate, membrane composition, and catalyst selectivity. The kinetic overpotentials for the OER and CO2RR also contribute to the total losses in the electrochemical cell.

Acid-Base Equilibria

The amount of carbon dioxide dissolved in the electrolyte depends on the pressure and temperature of the electrolyte. The equilibrium of CO_2 between gas and liquid phase,

$$CO_{2(g)} \rightleftharpoons CO_{2(aq)} \tag{11}$$

is given by the Henry's constant (K_0), such that

$$K_0 = \frac{c_{CO_2}}{f_{CO_2}} \tag{12}$$

where c_{CO_2} is the concentration of dissolved carbon dioxide, and f_{CO_2} is the fugacity of carbon dioxide in gas phase. The dependence of the Henry's constant on the temperature (T, in Kelvin) at ambient pressure is given as[16]

$$\ln(K_0) = 93.4517\left(\frac{100}{T}\right) - 60.2409 + 23.3585\ln\left(\frac{T}{100}\right) \tag{13}$$

The dissolved CO_2 can also be hydrated to form carbonic acid, but its concentration is only about 1/1000 of the concentration of dissolved CO_2.[17] Therefore, we do not distinguish between the hydrated and dissolved CO_2, and consider them as a single species. The dissolved CO_2 dissociates to produce bicarbonate and carbonate ions when pH is greater than 5. The corresponding pair of reactions is given as

$$CO_{2(aq)} + H_2O \underset{k_{-1}}{\overset{k_{+1}}{\rightleftharpoons}} H^+ + HCO_3^-, \quad pK_1 = 6.37 \tag{14}$$

$$HCO_3^- \underset{k_{-2}}{\overset{k_{+2}}{\rightleftharpoons}} H^+ + CO_3^{2-}, \quad pK_2 = 10.25 \tag{15}$$

The values of the forward rate constants of reactions (14) and (15) are $k_{+1} = 3.71\times10^{-2}\ s^{-1}$ and $k_{+2} = 59.44\ s^{-1}$, respectively.[18] The reverse rate constants can be obtained from pK_1 and pK_2 for reactions (14) and (15), respectively. The dependence of the equilibrium constants on temperature and salinity can be found elsewhere.[19] We also include the bulk ionization of water,

$$H_2O \underset{k_{-w}}{\overset{k_{+w}}{\rightleftharpoons}} H^+ + OH^- \tag{16}$$

The value of the forward rate constant of water ionization is $k_{+w} = 2.4\times10^{-5}\,\mathrm{mol\,L^{-1}\,s^{-1}}$ and the equilibrium constant is $K_w = 1\times10^{-14}\,\mathrm{mol^2\,L^{-2}}$.[20]

Transport of Species in the Electrolyte and Membrane

The transport of species in the electrolyte and membrane must satisfy mass conservation, such that

$$\frac{\partial c_i}{\partial t} + \frac{\partial N_i}{\partial x} = R_i \tag{17}$$

where N_i is the molar flux, and R_i is the volumetric rate of formation of species i (CO_2, HCO_3^-, CO_3^{2-}, H^+, and OH^-). The rate of production of species i, R_i, can be determined from reactions (14), (15), and (16). The molar flux of species in dilute electrolyte can be written as a sum of fluxes due to diffusion and migration.

$$N_i = -D_i \frac{\partial c_i}{\partial x} - z_i u_i F c_i \frac{\partial \phi_l}{\partial x} \tag{18}$$

where u_i is the mobility of ion given by the Nernst-Einstein relationship, and ϕ_l is the electrolyte potential. The diffusion coefficients of species in the dilute electrolyte are given in Table S 2. We neglect the variation of diffusion coefficients with the electrolyte concentration, as the variation is marginal for dilute electrolytes (<< 10 mol%).[21]

Table S 2 Diffusion coefficients of species in water at infinite dilution at 25℃ [22-23]

Species	**Diffusion Coefficient (10^{-9} m^2 s^{-1})**	**Mobility (10^{-7} m^2 V^{-1} s^{-1})**
CO_2	1.91	-
HCO_3^-	1.185	0.462
CO_3^{2-}	0.923	0.359
H^+	9.311	3.626
OH^-	5.273	2.054
K^+	1.957	0.762

The electrolyte current density i_l can be obtained from the total ionic flux,

$$i_l = F\sum_i z_i N_i \tag{19}$$

and the assumption of electro-neutrality,

$$\sum_i z_i c_i = 0 \tag{20}$$

The same set of Equations [(17)-(20)] were used to model the boundary layer region, the well-mixed region, and the membrane. Expressions for the rate of CO_2 transfer to or from the electrolyte, and diffusion coefficients for transport of ions through the membrane are discussed in the next three subsections.

Well-Mixed Electrolyte

The well-mixed region of the electrolyte was assumed to have no diffusional resistance and therefore charged species are transported only by migration. The net rate formation of HCO_3^-, CO_3^{2-}, H^+, OH^- were set to zero in the bulk because reactions(14), (15), and (16) were assumed to be at equilibrium. Therefore, only the rate of CO_2 transfer from gas phase to liquid phase was non-zero. A constant feed of CO_2 in the well-mixed region was included as an additional generation term on the right side of Equation (17), given as

$$R_{\mathrm{CO_2,\,feed}} = k_l a \left(K_0 f_{\mathrm{CO_2}} - c_{\mathrm{CO_2}} \right) \tag{21}$$

where $k_l a$ (s^{-1}) is the volumetric mass-transfer coefficient on the liquid side of gas-liquid interface, and $c_{\mathrm{CO_2}}$ (mol/m^3) is concentration of dissolved CO_2 in the bulk electrolyte. The value of mass transfer coefficient for CO_2 gas-liquid mass transfer in bicarbonate electrolyte is 1.75×10^{-5} m s^{-1}.[24] The boundary layer thickness of ~50 μm was chosen according to the limiting current density of CO2R.

Membrane

The anion exchange membrane (AEM) such as Selemion AMV was modeled as a solid electrolyte of 100 μm thickness with a fixed concentration of background positive charge of 1 M. The diffusion coefficients of anions and cations were reduced by a factor of 10^{13} and by a factor of 100 (assumed), respectively, relative to those in the liquid electrolyte.

Charge-Transfer Reactions at Anode and Cathode

The charge-transfer kinetics at the anode and cathode were modeled using the expression for Tafel kinetics, such as

$$i_s = i_l = i_R = i_0 \exp\left(\frac{\alpha F \eta}{RT}\right) \tag{22}$$

where i_s is the electrode current density, i_R is the reaction current density, i_0 is the exchange-current density, and α is the transfer coefficient. The kinetic overpotential of a catalyst is given by $\eta = \phi_s - \phi_l - E^0 + \Delta\phi_{\text{Nernstian}}$, where E^0 is the equilibrium potential of the half-reaction at standard condition and, ϕ_s is the electrode potential.

The half-cell reaction at the Pt anode is the oxidation of water, which creates acidic conditions near the electrode.

$$\mathrm{H_2O} \rightarrow \frac{1}{2}\mathrm{O_2} + 2\mathrm{H^+} + 2\mathrm{e^-}, \quad E^0 = 1.229\,\mathrm{V} \tag{23}$$

The other half-cell reactions on Ag cathode involve the reduction of carbon dioxide and water. As shown below, these reactions occur under alkaline conditions and, hence, can be written as:

$$\begin{aligned} 2\mathrm{H_2O} + 2\mathrm{e^-} &\rightarrow \mathrm{H_2} + 2\mathrm{OH^-} \qquad E^0 = 0\,\mathrm{V} \\ \mathrm{CO_2} + \ \mathrm{H_2O} + 2\mathrm{e^-} &\rightarrow \mathrm{CO} + 2\mathrm{OH^-} \qquad E^0 = -0.10\,\mathrm{V} \end{aligned} \tag{24}$$

The kinetic parameters for OER on Pt and CO2RR on Ag are given in Table S3. The kinetic parameters for OER on Pt were obtained from Birss and Damjanovic.[25]

Table S3: Tafel parameters for product-specific charge-transfer kinetics on Pt anode, Ag cathode

Reaction Products	**Catalyst**	i_0 **(mA cm^{-2})**	α
O_2	Pt	4.684×10^{-9}	0.500
CO	Ag	0.13393	0.00149

Electrode Current Density and Applied Potential

The current density at a metal electrode is given by Ohm's law:

$$i_s = -\kappa_s \frac{\partial \phi_s}{\partial x} \tag{25}$$

where κ_s is the conductivity of the electrode.

To maintain electroneutrality, the divergence of current density in the solid and the liquid must be zero:

$$\frac{\partial i_l}{\partial x} = 0, \quad \frac{\partial i_s}{\partial x} = 0 \tag{26}$$

The potential in the electrochemical cell was calculated relative to the zero potential of electrolyte at cathode-electrolyte interface. The potential of anode (solid) was set to 3.2 V. Equations (9)-(26) were solved using COMSOL Multiphysics 5.2a to study the distribution and reduction of CO_2 in a fully integrated AP system.

S8 Economic Analysis

To realize the feasibility of the integrated CO_2 capture and reduction processes discussed in this work, a detailed assessment of the material and operating costs was performed. This analysis was performed in three parts where the first part was to determine the cost of manufacturing one single photoelectrochemical (PEC) cell which can be used to reduce the captured CO_2 to CO, the second part was to determine the cost of operation of the CO_2 capture unit, and the third part was to calculate the cost of compressing and pumping the CO_2 from the carbon capture unit to the PEC units. Due to the difference in the nature and size of the CO_2 capture processes considered, the final economic data obtained were normalized to \$/ton CO_2 to get a better understanding of the performed economic analysis.

Cost of the PEC device

A crucial part of this analysis was to evaluate the quantity of the different components required for making a PEC device. The major components of a PEC device are a photo absorber, an anode, a cathode, and a membrane. A PEC device[26] of dimensions 1.2m X 1.7m consisting of a WO_3 photoabsorber, a silver nanofoam cathode (highly selective for CO production) a Nickel anode with the same amount of loading as the silver cathode, an AEM, and an acrylic chassis was chosen for the electrochemical CO_2 reduction. Table S4 shows the cost of the individual components and the total material cost the PEC device.

Table S4: Material costs for the components of the PEC device

Sr no	Material	Cost	Quantity	Total Cost	Source
1	WO_3	\$ 30/kg	13.15 kg	\$ 394.37	Alibaba
2	Nickel	\$ 15/kg	183.6 g ($10\ mg/cm^2$)[27]	\$ 2.75	Alibaba
3	Silver	\$ 502.77/kg	183.6 g ($10\ mg/cm^2$)[27]	\$ 92.31	Silverprice.org
4	AEM	\$ 31.25/m^2	0.184 m^2	\$ 5.74	Alibaba
5	Acrylic	\$3.80/kg	10 kg	\$ 38	Alibaba

The total cost of one PEC device is \$ 533.17.

Cost of operation of CO_2 capture units

The four CO_2 capture processes considered for the economic analysis are MEA, solid adsorption, electrodialysis and membrane capture. For a typical coal-fired power plant or direct CO_2 capture from air, the cost of operation ($/ton CO_2) for MEA, solid adsorption, and membrane capture is already available in the literature and is used here directly. Table S5 shows the cost of operation and operating conditions chosen for these processes. The cost of operation of electrodialysis was calculated by scaling up the experimental setup used by Eisaman et al.[15] to capture 1-ton CO_2/day.

Table S5: Cost of operation of various carbon capture technologies

Sr no	**Process**	**Absorbent/ Adsorbent**	**Energy Requirement (kJ/mol)**	**CO_2 capture rate (ton/day)**	**Source of CO_2**	**Feed CO_2 conc.**	**Cost ($/ton CO_2)**
1	Absorption	MEA	181	11.5	Flue gas	15%	49[10]
2	Adsorption	K_2CO_3	44.72	7.6	Flue gas	15%	57[7,10]
3	Membrane	Amine-based resin	190.94	1	Air	400 ppm	30[28]
4	Absorption	Electrodialysis	242	1	Seawater	400 ppm	394.41

The scaling up of the electrodialysis experimental setup described in section S4 was done by adding the repeating parallel units of the setup so that the whole system reaches the desired capacity of capturing 1-ton CO_2/day. One electrodialysis unit was scaled up to contain four times as many cells as the experimental setup (i.e., 36 cells, with a total flow rate of 24 lpm) Based on the flow rates of seawater and CO_2 being vacuum stripped at the same flow rate as its inlet flow rate, the total number of units needed to capture the desired capacity of CO_2 was calculated to by:

$$n_{ED} = \frac{F_{CO_2,reqd}}{F_{CO_2,ED}} \tag{27}$$

where n_{ED} is the number of electrodialysis units needed, $F_{CO2,reqd}$ is the flow rate of CO_2 required to be captured (1-ton/day or 0.263 mol/s), and $F_{CO2,ED}$ is the CO_2 flow rate in the seawater assuming the seawater has 400 ppm of CO_2. n_{ED} was calculated to be 7397. The cost of operation includes the cost of materials (Cu electrodes ($7.5/kg, source: Alibaba), membranes (Table S4), pumps ($20/pump, source: Alibaba)), assuming 2.5 years of life span for materials, and the cost of electricity (¢ 12/kWh). Each electrodialysis unit requires 2.2 kg Cu, 27 pieces of 180 cm^2 membranes, and one vacuum pump for stripping CO_2 from the acidic compartment. The total cost of operation is determined to be $394.41/ton CO_2.

Economic analysis of the integrated CO_2 capture and reduction systems

Due to the difference in the operation of different CO_2 capture technologies considered, there are two types of integrated systems defined as seen from Figure 1 of the manuscript. The integrated cascade system model is used for MEA, Adsorption, and Electrodialysis as it is not practically feasible to have a fully integrated system for these processes. The fully integrated system model is used for the membrane capture technique as the membrane can directly be attached at the back of a PEC device to make it a fully integrated system (Figure 1(C)). Figure S13 shows schematics of these two types of systems.

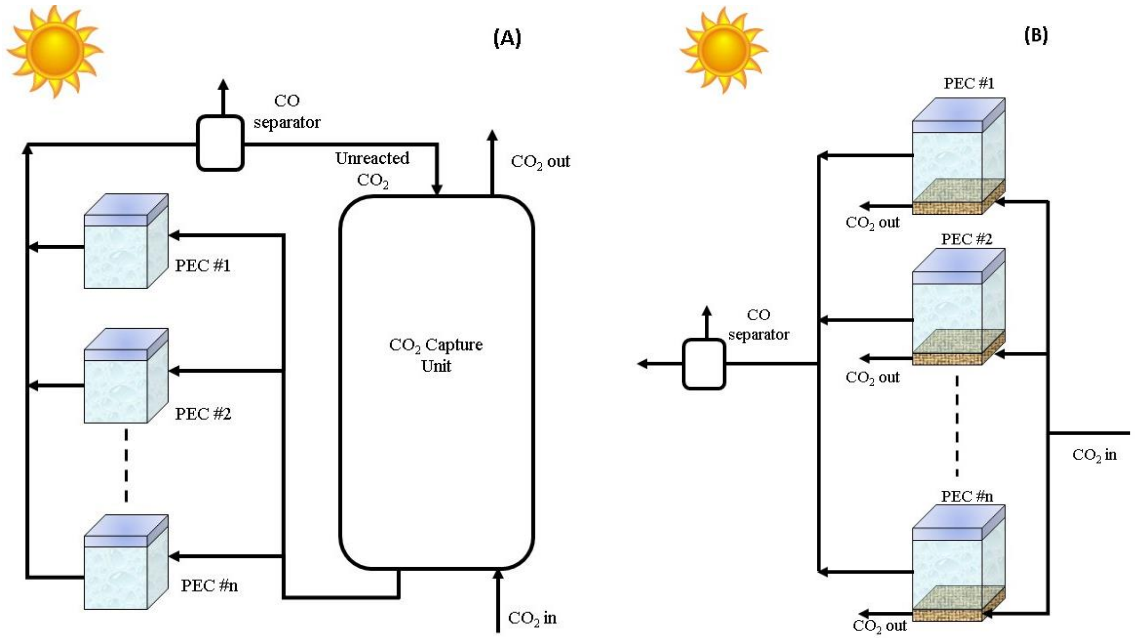

Figure S 13: Schematics of (A) the integrated cascade systems where the CO_2 is fed in to the carbon capture unit and the outlet stream containing the captured CO_2 is sent to n PEC devices where CO_2 gets reduced to CO and (B) the fully integrated system for membrane capture unit where CO_2 comes at the bottom (dry-side) of the unit and is released to the wet-side into the PEC where it gets reduced to CO.

To get the maximum CO_2 reduction out of each cell, the PEC was assumed to operate at the maximum efficiency with a current density of 12 mA/cm^2. The inlet into the PEC was assumed to be saturated with CO_2 (33mM). Polarization losses in an electrochemical cell reduce the efficiency of CO2RR and therefore to keep these losses minimum, the outlet concentration of CO_2 from PEC was taken to be 0.4 times the saturated concentration.[29] From this data the flow rate for each PEC device can be calculated by:

$$(C_{in} - C_{out})\dot{Q} = \frac{iA}{nF} \tag{28}$$

where C_{in} is the inlet concentration of CO_2 (33mM), C_{out} is the outlet concentration of CO_2 (13.2mM), $\dot{Q}$ is the flow rate (lit/s), i is the current density (mA/cm^2), A is the area, n is the number

of electrons transferred for the reaction (n=2), and F is the Faraday's constant. $\dot{Q}$ is calculated to be 0.06 lit/s. This is the optimal flow rate for one PEC device. The number of PEC devices needed can be obtained by equating the rate of CO_2 capture from the CO_2 capture unit to the rate of the recycle feed. Also, for integrated cascade systems, there is an additional capital and operation cost of pumps and compressors for transporting the captured CO_2 to the PEC units need to be included in the operation cost given in Table S5. A 5 lit/min capacity pump for each PEC unit ($ 20 per pump, source: Alibaba) and an 80kW 100 hp compressor per 100 PEC units ($ 8500 per compressor, source: Alibaba) are assumed to be sufficient and are accounted for in the cost of operation. Since the number of units is different for each of the CO_2 capture processes, a brief explanation on each of the calculations for each of the processes is given below.

MEA

For a typical 400 MW coal-fired power plant, the flue gas exhaust has a CO_2 flow rate of 1.5 kmol/s. An industrial MEA CO_2 capture unit with a contact area of 2000 m^2 and a CO_2 capture capacity of 1.52 mmol/m^2 s. [6] The rate of CO_2 capture can be calculated by:

$$r_{CO2} = N_{CO_2} \times A \tag{29}$$

where r_{CO2} is the rate of CO_2 capture (mol/s), N_{CO2} is the capture capacity, and A is the area of contact. From equation (29) we can calculate r_{CO2} to be 3.04 mol/s (or 68.24 lit/s). The number of PEC units required can now be calculated by using the following equation.

$$n_{PEC} = \frac{r_{CO2}(\text{in lit/s})}{\dot{Q}} \tag{30}$$

where n_{PEC} is the number of PEC units. About 1184 PEC units would be required to be operated in parallel so that the flow rate of the recycle stream is the same as the rate of CO_2 captured. The total cost of the PEC units can be calculated by:

$$C_{total,PEC} = C_{PEC} \times n_{PEC} \tag{31}$$

where $C_{total,PEC}$ and C_{PEC} are the total cost ($) and the cost of one PEC unit respectively. It is assumed that all the CO_2 dissolved in the inlet stream of PEC gets converted to CO before the polarization losses become dominant and reduce the efficiency of the PEC unit (0.6 mol CO formed/ mol of CO_2). The term on the right-hand side of equation (28) gives us the rate of formation of CO in mol/s. This can be used to calculate the total amount of CO formed in a year and the amount of CO_2 utilized by the PEC units. the total cost per ton of CO_2 is determined by the following equation.

$$C_{total} = C_{op} + C_{pump} + \frac{C_{total,PEC}}{m_{CO_2} \times t_L} \tag{32}$$

where C_{total} is the total cost in $/ton CO_2, C_{op} is the cost of operation of the CO_2 capture process ($/ton CO_2) taken from Table S5, m_{CO2} is the total mass of CO_2 utilized in a year (ton/yr), and t_L is the lifetime of the PEC units (5 years), and C_{pump} is the total cost of pumping and compression based on the number of PEC units required. The total cost was calculated to be $ 156.94 /ton CO_2.

For every ton of CO_2 consumed 0.38 ton of CO is formed (0.6 mols of CO_2 converted to CO). Therefore, the total cost in $/ton CO can be calculated by:

$$C_{total,CO} = \frac{C_{total}}{x_{CO}} \tag{33}$$

where $C_{total,CO}$ is the total cost in $/ton CO, and x_{CO} is the ratio of ton of CO formed to the ton of CO_2.

Adsorption

The economic analysis for the adsorption process was similar to that of MEA. The exhaust flue gas is fed into the fluidized bed column carrying 0.1 ton of solid adsorbent captures CO_2 at the rate of 2 mol/s and therefore requires about 779 PEC units (using equation (30)). The total cost, calculated under the assumption of complete conversion of dissolved before the polarization losses start increasing due to the drop in CO_2 concentration using equations (31) and (32), is $154.42/ ton CO_2.

Electrodialysis

The number of electrodialysis units required to capture 1-ton CO_2/day was determined to be 7397 using equation (27). The maximum flow rate at which CO_2 is stripped was given as 0.3 lit/min.[15] Therefore, the total flow rate of this stripped CO_2 going into the PECs would be:

$$\dot{Q}_{total} = n_{ED} \times \dot{Q}_{CO2} \tag{34}$$

where $\dot{Q}_{total}$ is the total flow rate (lit/min), n_{ED} is the number of electrodialysis units, and $\dot{Q}_{CO2}$ is the flow rate of stripped CO_2 (lit/min). $\dot{Q}_{total}$ should be equal to the total flow rate from the PEC devices. Therefore, the total number of PEC units is calculated to be 107 using equation (30). Using equations (31) and (32), the total cost obtained was $423.81 / ton CO_2.

Membrane capture

Lackner's[14] prototype design for membrane capture from air was taken for the economic analysis for the fully integrated CO_2 capture and reduction system. For a capacity of 1-ton CO_2/day with the air velocity of 1 m/s there are 60 units of membrane required. Since this is a fully integrated system as seen from Figure S13, the number of PEC units required will also be 60. The total cost is calculated to be $70.39/ton CO_2 using equations (31) and (32) with C_{pump} to be 0 for a fully integrated system.

Using equation (33) the cost of production of CO ($/ ton CO) was calculated and a comparison of all the different integrated systems is shown in Table S6. Case 4 in Table S6 takes into account the pumping and the compression costs for the membrane capture technology as it is treated as a cascaded process. These costs are not added to the total cost of operation in case 5 which shows a much lower cost of operation for a fully integrated system.

Table S6: Cost of CO production from different Integrated AP systems

Sr no	**Process**	**$/ ton CO**	**Ton CO/day**	**PEC Land Area (m^2)**
1	Absorption: MEA (Cascade)	413.02	4.41	2415.36
2	Adsorption: K_2CO_3 (Cascade)	406.36	2.91	1589.16
3	Absorption: Electrodialysis (Cascade)	1395	0.38	218.28
4	Membrane: Amine-based resin (Cascade)	325.5	0.38	122.40
5	Membrane: Amine-based resin (Fully Integrated)	185.24	0.38	122.40

References:

1. Henry, C. H., Limiting efficiencies of ideal single and multiple energy gap terrestrial solar cells. *J. Appl. Phys.* **1980,** *51* (8), 4494-4500.
2. Singh, M. R.; Clark, E. L.; Bell, A. T., Thermodynamic and achievable efficiencies for solar-driven electrochemical reduction of carbon dioxide to transportation fuels. *Proc. Natl. Acad. Sci.* **2015,** *112* (45), E6111-E6118.
3. Karam, N. H.; King, R. R.; Cavicchi, B. T.; Krut, D. D.; Ermer, J. H.; Haddad, M.; Cai, L.; Joslin, D. E.; Takahashi, M.; Eldredge, J. W., Development and characterization of high-efficiency GaInP/GaAs/Ge dual-and triple-junction solar cells. *IEEE Trans. Electron Devices* **1999,** *46* (10), 2116-2125.
4. Keith, D. W.; Ha-Duong, M.; Stolaroff, J. K., Climate strategy with CO_2 capture from the air. *Clim. Change* **2006,** *74* (1-3), 17-45.
5. Lv, B.; Guo, B.; Zhou, Z.; Jing, G., Mechanisms of CO_2 capture into monoethanolamine solution with different CO_2 loading during the absorption/desorption processes. *Environ. Sci. Technol.* **2015,** *49* (17), 10728-10735.
6. Yuan, Y.; Rochelle, G. T., CO_2 absorption rate in semi-aqueous monoethanolamine. *Chem. Eng. Sci.* **2018,** *182*, 56-66.
7. Samanta, A.; Zhao, A.; Shimizu, G. K.; Sarkar, P.; Gupta, R., Post-combustion CO_2 capture using solid sorbents: a review. *Ind. Eng. Chem. Res.* **2011,** *51* (4), 1438-1463.
8. Prajapati, A.; Renganathan, T.; Krishnaiah, K., Kinetic Studies of CO_2 Capture Using K2CO3/Activated Carbon in Fluidized Bed Reactor. *Energy Fuels* **2016,** *30* (12), 10758-10769.
9. Duan, Y.; Luebke, D.; Pennline, H. H., Efficient theoretical screening of solid sorbents for CO2 capture applications. *Int. J. Clean Coal Energy* **2012,** *1* (01), 1.
10. Ho, M. T.; Allinson, G. W.; Wiley, D. E., Reducing the cost of CO_2 capture from flue gases using pressure swing adsorption. *Ind. Eng. Chem. Res.* **2008,** *47* (14), 4883-4890.
11. Wang, T.; Lackner, K. S.; Wright, A., Moisture swing sorbent for carbon dioxide capture from ambient air. *Environ. Sci. Technol.* **2011,** *45* (15), 6670-6675.
12. Le, X. T., Permselectivity and microstructure of anion exchange membranes. *J. Colloid Interface Sci.* **2008,** *325* (1), 215-222.
13. Kiss, A. M.; Myles, T. D.; Grew, K. N.; Peracchio, A. A.; Nelson, G. J.; Chiu, W. K., Carbonate and bicarbonate ion transport in alkaline anion exchange membranes. *J. Electrochem. Soc.* **2013,** *160* (9), F994-F999.
14. Lackner, K. S., Capture of carbon dioxide from ambient air. *Eur. Phys. J. Spec. Top.* **2009,** *176* (1), 93-106.
15. Eisaman, M. D.; Parajuly, K.; Tuganov, A.; Eldershaw, C.; Chang, N. R.; Littau, K. A., CO_2 extraction from seawater using bipolar membrane electrodialysis. *Energy Environ. Sci.* **2012,** *5* (6), 7346-7352.
16. Riebesell, U.; Fabry, V. J.; Hansson, L.; Gattuso, J.-P., *Guide to best practices for ocean acidification research and data reporting*. Office for Official Publications of the European Communities: 2011.
17. Soli, A. L.; Byrne, R. H., CO_2 system hydration and dehydration kinetics and the equilibrium CO_2/H_2CO_3 ratio in aqueous NaCl solution. *Mar. Chem.* **2002,** *78* (2), 65-73.
18. Schulz, K. G.; Riebesell, U.; Rost, B.; Thoms, S.; Zeebe, R., Determination of the rate constants for the carbon dioxide to bicarbonate inter-conversion in pH-buffered seawater systems. *Mar. Chem.* **2006,** *100* (1), 53-65.

19. Riebesell, U.; Fabry, V. J.; Hansson, L.; Gattuso, J.-P., *Guide to best practices for ocean acidification research and data reporting*. Publications Office of the European Union Luxembourg: 2010.
20. Atkins, P.; De Paula, J., *Atkins' physical chemistry*. Oxford University Press: 2014.
21. Newman, J.; Thomas-Alyea, K. E., *Electrochemical systems*. John Wiley & Sons: 2012.
22. Flury, M.; Gimmi, T. F., Solute Diffusion. *Methods of Soil Analysis: Part 4 Physical Methods* **2002,** (methodsofsoilan4), 1323-1351.
23. Jähne, B.; Heinz, G.; Dietrich, W., Measurement of the diffusion coefficients of sparingly soluble gases in water. *J. Geophys. Res.: Oceans (1978–2012)* **1987,** *92* (C10), 10767-10776.
24. Cents, A.; Brilman, D.; Versteeg, G., CO_2 absorption in carbonate/bicarbonate solutions: The Danckwerts-criterion revisited. *Chem. Eng. Sci.* **2005,** *60* (21), 5830-5835.
25. Birss, V. I.; Damjanovic, A., A study of the anomalous pH dependence of the oxygen evolution reaction at platinum electrodes in acid solutions. *J. Electrochem. Soc.* **1983,** *130* (8), 1694-1699.
26. Sathre, R.; Scown, C. D.; Morrow, W. R.; Stevens, J. C.; Sharp, I. D.; Ager, J. W.; Walczak, K.; Houle, F. A.; Greenblatt, J. B., Life-cycle net energy assessment of large-scale hydrogen production via photoelectrochemical water splitting. *Energy Environ. Sci.* **2014,** *7* (10), 3264-3278.
27. Rosen, J.; Hutchings, G. S.; Lu, Q.; Rivera, S.; Zhou, Y.; Vlachos, D. G.; Jiao, F., Mechanistic insights into the electrochemical reduction of CO_2 to CO on nanostructured Ag surfaces. *ACS Catal.* **2015,** *5* (7), 4293-4299.
28. Sanz-Perez, E. S.; Murdock, C. R.; Didas, S. A.; Jones, C. W., Direct capture of CO_2 from ambient air. *Chem. Rev.* **2016,** *116* (19), 11840-11876.
29. Singh, M. R.; Clark, E. L.; Bell, A. T., Effects of electrolyte, catalyst, and membrane composition and operating conditions on the performance of solar-driven electrochemical reduction of carbon dioxide. *PCCP* **2015,** *17* (29), 18924-18936.
30. Liu, C.; Colón, B. C.; Ziesack, M.; Silver, P. A.; Nocera, D. G., Water splitting–biosynthetic system with CO_2 reduction efficiencies exceeding photosynthesis. *Sci* **2016,** *352* (6290), 1210-1213.